Research Square

Preprints are preliminary reports that have not undergone peer review.
They should not be considered conclusive, used to inform clinical practice,
or referenced by the media as validated information.

Asymmetric Triple-Channel Schottky Barrier FinFET Biosensor for Cardiac Biomarker Detection

Radhika P[1]
Vellore Institute of Technology
K Lakshita
Vellore Institute of Technology
Shalini Virumandi[2]
Vellore Institute of Technology
Prayag Sharma[3]
Vellore Institute of Technology
Ravi Tiwari[1]
Vellore Institute of Technology
Prashanth Kumar
prashanthkumar.b@vit.ac.in
Vellore Institute of Technology

Research Article

Keywords: Biosensor, cardiac biomarkers, FinFET, Schottky barrier, dielectric modulation, SiC, triple-channel architecture

Posted Date: November 6th, 2026

DOI: https://doi.org/10.21203/rs.3.rs-11230907/v1

License: This work is licensed under a Creative Commons Attribution 4.0 International License.
Read Full License

Additional Declarations: No competing interests reported.

Asymmetric Triple-Channel Schottky Barrier FinFET Biosensor for Cardiac Biomarker Detection

Radhika P[1], Lakshita K J[1], Shalini Virumandi[2], Prayag Sharma[3], Ravi Tiwari[1], Prashanth Kumar*[1]
[1]School of Electronics Engineering, Vellore Institute of Technology Chennai, Tamil Nadu, 600127, India.
[2]School of Advanced Sciences, Department of Physics, Vellore Institute of Technology Chennai, Tamil Nadu, 600127, India.
[3]School of Computer Science and Engineering, Vellore Institute of Technology Chennai, 600127, India.
*corresponding author mail id: prashanthkumar.b@vit.ac.in

Co-authors mail.id: radhikapalakkal1@gmail.com,kj.lakshita@gmail.com, shalinideva2700@gmail.com, prayagsharma2648@gmail.com, ravitiwari.tiwariravi@gmail.com

Abstract

We have designed and simulated a new form of Schottky barrier FinFET, known as an SB-FinFET, that is designed to detect cardiac biomarker proteins without labels. The SB-FinFET uses an asymmetric, triple-channel stacked architecture, with the three channels positioned vertically on top of each other. The SB-FinFET consists of three channels made of silicon carbide (SiC), with nickel silicide (NiSi) Schottky contacts and hafnium oxide (HfO_2) insulating material as the gate dielectric to reduce the amount of intrinsic leakage current and improve the efficiency with which electrostatic coupling occurs. The architecture allows for the decoupling of current driving ability from sensing ability because of the difference in doping levels of the channels: the two outer channels have a doping density of 1 x 10^{17} cm^{-3} and are 4 nm deep, while the central channel has a doping density of 1 x 10^{10} cm^{-3} and is 1 nm thick. The two outer channels provide a suitable amount of current drive and gain, while the central channel serves as a high-sensitivity transducer that converts the biomarker/protein interaction into an electrical signal. The 3D TCAD simulation results exhibit an I_{ON}/I_{OFF} ratio of approximately 1 x 10^8 with low subthreshold swing for target biomolecules that have dielectric constants within the range of k = 1.5–3.5 (e.g., uricase, streptavidin, and troponin). The performance was further characterized through an analysis of linearity with transconductance (g_m) and through third-order nonlinearity metrics (VIP_3 and IIP_3). The SB-FinFET has been compared against other types of devices, including Negative Capacitance FET (NC-FET) and Tunnel FETs (TFETs), for sensitivity and complexities associated with fabrication. The results from these comparisons show that SB-FinFET's performance is similar to the two other device structures previously mentioned, while having a lower complexity and cost to fabricate them. The SB-FinFET is therefore an excellent experimental platform for developing new cardiac diagnostics devices that would allow for rapid diagnosis at or near the site of patient care.

Keywords: Biosensor, cardiac biomarkers, FinFET, Schottky barrier, dielectric modulation, SiC, triple-channel architecture.

I. INTRODUCTION

According to the World Health Organization, cardiovascular diseases (CVDs) are one of the leading causes of death across the world, resulting in nearly 19.8 million deaths annually according to the World Health Organization[1]. Hence, the early and accurate detection of biomolecules that lead to these diseases - Troponin I/T, Myoglobin, Creatine Kinase-MB (CK-MB), and B-type Natriuretic Peptide (BNP) - is vital for timely intervention as would be required to prevent casualties due to myocardial infarction, heart failure and other heart diseases [2]. Traditional diagnostic methods such as enzyme-linked immunosorbent assay (commonly known as ELISA, and other laboratory-based immunoassays, are slow (turnaround time of 2-4 hours) and need specialized lab equipment, resulting in high operational costs and an inability to provide real-time monitoring [3-4]. This means, that although they are highly accurate, their limitations are a crippling factor in emergency medicine, resource-limited settings and delay clinical decisions in ways that affect patient survival. Therefore, as an alternative to such techniques, the Field-effect transistor (FET) based biosensors emerged, with promising features like label-free and real time detection, high sensitivity and miniaturization, as well as compatibility with CMOS technology for low-cost mass production, as can be seen in some works of literature [5- 7]. These devices operate on the principle that target biomolecules bound to nanoscale cavity regions between the gate electrode and the semiconductor channel, change the surface potential such that the channel conductance is affected, a phenomenon known as dielectric modulation [8-10] which is the skeleton of several such biosensors, including the one presented in this work. Among various FET architectures, the fin field-effect transistor (FinFET) has emerged as an excellent alternative due to its three-dimensional multi-gate structure that provides superior electrostatic control over the channel, reduced short-channel effects, and increased surface area for biomolecule capture compared to planar devices [11-14]. These modifications allow for potentially improved sensitivity. There have been many recent advances in biosensing using FinFETs (fin field effect transistors). This includes numerous studies which show the advantages of using nanocavities to create dielectric modulation in order to achieve improved sensitivity while utilizing this technology to measure biomolecules. For example, GaAs (Gallium Arsenide)-based FinFETs with a cavity (nanocavity) located below the gate have been simulated at the same time as actual experimental devices (organic risk and toxicity testing) to demonstrate that by simply changing the dielectric constant of the cavity, the measured threshold voltages and drain current of FinFETs will change due to an increase in the electric field coupling between the biomolecule and the gate [15]. Similarly, studies on under-gate junction-less finFET highlight the importance of careful geometric tuning of cavity dimensions and oxide thickness to improve sensitivity [16]. However, such studies primarily focus on ohmic-contact devices which are limited by degraded on-currents and more leakage. However, some critical challenges faced by conventional finFET biosensors with ohmic contacts limit their practical deployment for cardiac biomarker detection. Firstly, they offer less than optimal sensitivity due to the current-sensitivity trade-off. Light channel doping and thin body dimensions are important to maximize gate control, but lead to reduced on-currents, less than 10^{-7}A [17-19]. Meanwhile, optimizing for higher drive current with heavier doping or thicker channels leads to a compromise in sensitivity, especially for biomolecules with similar dielectric constants. Next, conventional silicon-channel devices have elevated off-state leakage currents ($I_{OFF} \sim 10^{-11}$ to 10^{-9} A). This can be due to short channel effects [20-21], and cause degraded the signal-to-noise ratio (SNR) beside an increase in the minimum detectable biomolecule concentration. In particular, this problem is worse for cardiac biomarkers, since they have relatively low dielectric constants (k = 1.5-3.5), which means smaller threshold voltage shifts that can be masked by noise. In an attempt to combat this, partial cavity models have been used to investigate low k biomarkers. For example, an analysis of the effects of steric hindrance in junction-less FinFET biosensors demonstrated that incomplete cavity filling leads to a reduction in sensitivity, especially for biomolecules with $k < 4$ [22]. Dielectric-modulated FinFETs have been tested like standard Field Effect Transistors (FETs) both dry and wet. In wet conditions, variations in the dielectric material due to moisture can dominate any potential intrinsic electrical responses, causing problems when trying to identify and differentiate between biomarkers with certainty. As a result of this work, it is critical that dielectric regions of operation be defined in order to provide useable results, especially where dielectric constants are very close to one another like with cardiac biomarkers. Modifications made to the FinFET through innovation have resulted in new designs and prototypes being created due to both high gate

current leakage and complex construction methods, including junction-less biosensors that have lower leakage rates, truncated-fin GaAs devices that limit current flow, and inverted-T structures that provide 40% improved sensitivity via better distribution of electric fields. Nevertheless, each of these prototype devices still consists of essentially uniform channels with only ohmic contacts, precluding the ability to independently adjust the sensitivity of each of these devices in relation to their current density.

While there have been many developments in advanced architectures such as negative capacitance FinFETs (NC-FinFETs) which provide a superior sub-threshold voltage control than their predecessor architectures, the manufacture of NC-FinFETs is still hindered due to the complexity of their manufacturing process and how precise the ferroelectric materials must be deposited and annealed. Furthermore, the reliability of NC-FinFETs is in question because there are no guarantees of their stable operation as there could be instability with the construction of an NC-FinFET. One example of this is the NC-FinFET biosensor with an MFIS gate stack that utilizes $HfZrO_2$ as the oxide layer (dielectric) which provided improved transconductance and sub-threshold performance than a traditional FinFET; however, the reliability tests for NC-FinFETs indicate that the devices are sensitive to fabrication variations, surface imperfections, and degradation from their ferroelectric dielectric; therefore, the reliability and repeatability of NC-FinFETs are still suspect. These reasons have led us to pursue alternative design architectures that can achieve similar electrical performance advantages. Reliable operation of a biosensor also involves using linear and stable bias conditions in addition to structural optimization. Research examining non-linear distortion mechanisms within FinFET biosensors has identified biasing conditions that provide the lowest amount of higher order transconductance terms in order to maintain smooth conduction and low distortion performance when measuring bio-chemical signals [23]. Maintaining a constant gate biasing condition would be advantageous to achieving this end. Another limitation is that majority of biosensor research has focused exclusively on high-k biomedical molecules with biosensor designs optimized for a broad range of dielectric constants (ranging from 2 to 12). Specific requirements relating to the analysis of cardiac biomarkers (using dielectrics from 1.5 to 3) remains largely unexplored in terms of the required device characteristics [6, 24].

Researchers have been looking for ways to overcome many of the barriers to efficient biosensing applications using Schottky barrier field-effect transistors (SB-FETs). For example, when using metal-semiconductor junctions in Schottky FETs, the need for excessive doping is removed so that the fabrication process is made simpler and more compatible with CMOS technology. Furthermore, the current rectification characteristics of Schottky barriers create a thermionic emission, which in turn reduces the off-state leakage current through the device; they will subsequently create a much larger SNR (signal-to-noise ratio) than currently possible[25-27].Other characteristics of Schottky barriers, including variations in the barrier height and width, will alter the gate potential of the device; this will change the effective oxide thickness (EOT) of the device and amplify the detection signal[28]. Despite the advantages of SB-FETs over traditional transistors for use in biosensing applications, there are several primary gaps in research regarding the implementation of SB-FETs for this application. For example, while SB-FETs have been studied extensively for construction of logic circuits and analog circuits, they have received only minor work during consideration for use in biosensing applications [29]. Specifically, a recent paper evaluating Ga_2O_3 vertical FinFETs with integrated Schottky barrier diodes, discussed the role of contact engineering in obtaining low on-resistance conduction through the devices [30-32]. In addition to the above study, papers discussing the concepts of barrier height modulation found in dual metal TFETs and in dielectric modulated DMDG TFET biosensors suggest that using Schottky barriers' modulation of height and width will also create a significantly increased SNR for the biosensors. However, to date, there is very limited research on the modulation of barrier height and width of SB-FETs, with respect to FinFET biosensors[33].

Additionally, Schottky barriers' current rectification characteristics naturally reduce off-state leakage when reverse-biased due to reduced thermionic emission, resulting in I_{OFF} values for Schottky barriers that are several orders of magnitude less than for conventional devices [34]. Schottky barriers' ability to modulate their barrier height and width with the applied gate potential allows for amplification of the detection signal by changing the effective oxide thickness (EOT) that biomolecules in the cavity will be subject to [35]. In addition, there are numerous advantages to using wide-bandgap semiconductors such as SiC over conventional Si channels, however, there has yet to be any investigation of SiC as a biosensor. The 6H polytype of SiC has an energy bandgap of 3.03 eV at 300 K. SiC also has 10^6 lower

intrinsic carrier concentrations than Si at room temperature (ni ~ 10^{-5} cm^{-3} vs. 10^{10} cm^{-3}), which indicates a large reduction in the diffusion currents that occur and also lower off-state leakage [36]. Supporting this, SiC is considered chemically stable and biocompatible, which provides an advantage when used in the highly corrosive biological fluid environments of body tissues [37]. Unfortunately, there is very little research published in academic journals about these sensors being used as biosensors in FinFET formats; therefore, design strategies such as an asymmetric multi-channel architecture that incorporates multiple parallel channels of varying widths or doping profiles have not been investigated as potential methods to meet the dual requirements of achieving high current drive with improved sensitivity. The review of current literature shows that there are many opportunities to innovate. The first is that there is a need for biosensor architectures to be optimized for the unique dielectric properties of low-k cardiac biomarkers. The second is that the use of Schottky barrier FinFETs has not been previously explored as a potential method to create biosensors with improved sensitivity through better barrier modulation. The third is that asymmetric multi-channel designs may offer an uncharted avenue for optimizing sensitivity without sacrificing current drive to produce biosensors with the high-performance standards needed for clinical cardiac diagnostics.

This work introduces a comprehensive analysis on dielectric-modulated Schottky barrier FinFET biosensors, which have been optimized especially for detecting cardiac biomarkers and other key proteins (such as uricase and streptavidin) with dielectric constant (k) values of between 1.5 and 3.5 [38]. The proposed device contains four innovative features: (i) Nickel Silicide (NiSi) Schottky contacts that create an optimal barrier height (~0.9eV) with the n-type SiC channel to limit leakage currents while providing sufficient ON-state current, (ii) a 6H-SiC wide bandgap channel to limit the generation of intrinsic carriers and diffusion currents, (iii) a high-k Hafnium Oxide (HfO_2) gate dielectric providing superior electrostatic coupling, and (iv) a new asymmetrical triple channel design featuring two highly doped outer channels (4 nm width; 10^{17} cm^{-3} dopant concentration) carrying high drive current while the centrally located lightly doped channel (1 nm width; 10^{10} cm^{-3} dopant concentration) acts as an ultra-sensitive biosensor. By achieving balance between current drive and sensitivity, this device will allow for the simultaneous optimization of both parameters. In addition, this work systematically studies these types of devices for dielectric controlled biosensing applications focused on the range of dielectric constants applicable to cardiac markers. Detailed three-dimensional simulations using physics-based modeling in the Synopsys Sentaurus TCAD tool have been performed on the proposed SB-FinFET biosensor device design and the results of those simulations show that the proposed biosensor achieves the following: (i) I_{ON}/I_{OFF} ratio exceeding 10^8 in the cardiac biomarker dielectric range (k = 1.5-3.5), which represents over an order of magnitude improvement as compared to previous FinFET biosensors, (ii) device performance at the level of other published NC-FinFETs, Tunnel FETs and Junction-less devices, (iii) subthreshold swing (SS) approaching that predicted by thermionic emission, (iv) increased fabrication simplicity because there is no longer a requirement for ultra-heavy doping. The results produced during our research include DC transfer characteristics (I_D-V_G), transconductance (g_m) and linearity metrics (VIP_2, VIP_3, IIP_3), a sensitivity analysis that identifies the effect of varying the cavity fill factor on sensor performance and a demonstration of the effects of channel doping polarity (n-type versus p-type) on biomolecule detection sensitivity in order to show that the SB-FinFET device can provide distinct identification for biomolecules with closely spaced dielectric constants. The paper is divided into five sections; Section 2 describes the TCAD device design and results validating the TCAD simulation methods, Section 3 presents electrical performance and sensitivity benchmarking of the device, Section 4 discusses the mechanisms used to achieve those electrical characteristics as well as the diagnostics that can be performed to verify the mechanisms and the results of those diagnostics are summarized in Section 5.

II. Device Structure

The stepwise fabrication process of the proposed FinFET structure is illustrated in Fig. 1 (a–g). The process begins with the formation of the silicon substrate, which acts as the mechanical and electrical foundation of the device, as shown in Fig. 1(a). Subsequently, a buried oxide (BOX) layer is deposited over the substrate to establish a silicon-on-insulator platform that provides electrical isolation between

the active device region and the bulk substrate, as depicted in Fig. 1(b). Following the formation of the BOX layer, the source and drain regions are defined on the oxide surface through appropriate patterning and material deposition, leaving a narrow spacing between them for channel formation, as illustrated in Fig. 1(c). In the next step, an initial channel region (C1) is introduced between the source and drain terminals to establish the conduction path for carrier transport, as shown in Fig. 1(d). To enhance the conduction characteristics and improve channel control, a second channel region (C2) is incorporated adjacent to the first channel between the source and drain electrodes, resulting in a dual-channel configuration, as depicted in Fig. 1(e). Subsequently, the channel regions are shaped into vertical fin-like structures, forming the characteristic multi-fin architecture of the FinFET device, as presented in Fig. 1(f). These fins increase the effective channel width and enable improved electrostatic control over the carriers. Finally, a gate oxide layer is deposited around the fin structures followed by the formation of the gate electrode, which wraps around the channel region to establish a tri-gate configuration, as illustrated in Fig. 1(g). This three-dimensional gate structure provides superior gate-to-channel coupling, thereby suppressing short-channel effects and enhancing the overall device performance compared to conventional planar transistor architectures. The proposed device is a three-dimensional asymmetric triple-channel Schottky-barrier FinFET biosensor, intended to provide of robust electrostatic control, suppression of short-channel effects, and dielectric modulation sensitivity with nanometer-scale dimensions. Fig.1(h) presents a three-dimensional schematic view of the complete device structure.

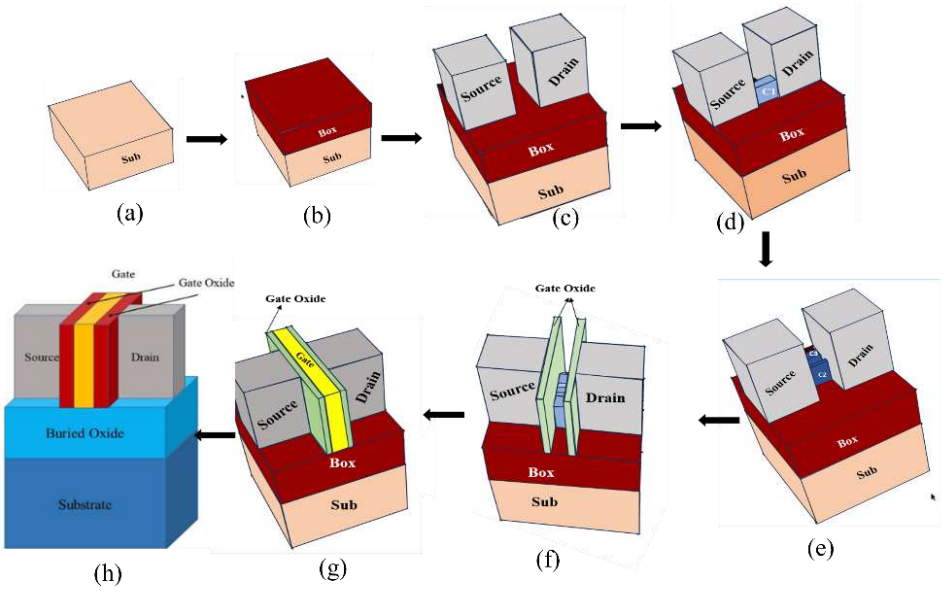


Fig. 1. Stepwise fabrication of the proposed FinFET structure: (a) substrate formation, (b) BOX layer deposition, (c) source/drain formation, (d) first channel (C1) introduction, (e) second channel (C2) formation, (f) fin and gate oxide formation, (g) gate electrode formation and (h) The completed device structure, illustrating the source, drain, gate, gate oxide, buried oxide, and substrate layers.

This device is made using a 50 nm × 50 nm × 30 nm silicon-on-insulator (SOI) substrate platform (refer table 1 for dimensions of the structure), with an embedded 20 nm buried oxide layer of thermally grown SiO_2 (κ = 3.9). The substrate is made of undoped silicon, which prevents parasitic leakage and electrostatic coupling, thereby localizing the sensing mechanism to the Schottky-contacted channel and suppressing back-gate coupling and leakage effects that could degrade the SNR. Nickel silicide (NiSi) is used as a material for source and drain contacts to create a Schottky junction with the semiconductor channel. NiSi was chosen due to its reduced thermal budget, lower resistivity, and its lack of limitations in smaller dimension applications [39].

As discussed earlier, the energy bandgap, intrinsic carrier concentration and biocompatibility of 6H-

SiC makes it an excellent choice for channel material. 6H–SiC as an example have much larger critical electric strengths than most other semiconductors [24]. As such, 6H–SiC polytypes are more resistant to Electric Field Induced Breakdown, even with aggressive Gate Length Scaling (10 nm) in this design. In contrast, while the lower ~60 $cm^2/V \cdot s$ electron mobility of 6H-SiC compared to ~1400 $cm^2/V \cdot s$ of silicon does result in lower absolute current levels, this trade-off is acceptable for biosensing where noise immunity and detection sensitivity are more important than switching speeds. In addition, the device results of this research demonstrate that the lower electron mobility of 6H-SiC does not affect the overall performance of the device due to the very large transconductance (10-5 μS). The electron affinity for 6H-SiC is 3.45 eV [28, 29] and the work function for NiSi can be estimated at 4.4 eV [30]. This gives a barrier height of approximately 0.95 eV, which is designed to limit I_{OFF} (~10-15 A) due to thermionic emission when the thickness of the barrier is reduced by applying positive gate bias and allowing robust thermionic–field emission .

Table 1: Structure dimensions

S.No.	Parameter	Value
1	Substrate length	50 nm
2	Substrate width	50 nm
3	Substrate thickness	30 nm
4	BOX (oxide) thickness	20 nm
5	Source length	20 nm
6	Source width	20 nm
7	Source height	30 nm
8	Drain length	20 nm
9	Drain width	20 nm
10	Drain height	30 nm
11	Channel length	10 nm
12	Channel width (Channel 1)	4 nm
13	Channel width (Channel 2)	1 nm
14	Channel width (Channel 3)	4 nm
15	Channel height	10 nm
16	Gate oxide (each side) thickness	2 nm
17	Gate electrode width	6 nm
18	Gate electrode height	30 nm
19	Cavity length	10 nm
20	Cavity width	20 nm
21	Cavity height	20 nm

One key aspect of the innovative Biosensor is the presence of three independent channels, or compartments, comprised of silicon carbide (SiC) nanosheets that differ in structural characteristics as can be seen in Figure 2b. Each of these channels functions independently of each other and thus can simultaneously satisfy the two conflicting electrical properties needed; a large drive current that can yield reliable readings ($I_{ON} > 10^{-6}$ A) and a very sensitive channel (Channel 2) that possesses a very large response to small changes in surface potential triggered by the attachment of biomolecules to the surface of the channel. As previously mentioned, the three channels of the biosensor are made of SiC nanosheets, with the outer two channels (Channels 1 and 3) having a length of 10 nm, a height of 10 nm, a width of 4 nm, and a moderate doping level of 1×10^{17} cm^{-3} of arsenic. The outer two channels provide low-resistance pathways for current (providing a large I_{ON}) while allowing for rapid transient response due to the large amounts of drive current available to them. In contrast, the central channel (Channel 2), has a length of 10 nm, a height of 10 nm, and a width of 1 nm, and is doped at a very low concentration of 1×10^{7} cm^{-3} of arsenic. As indicated in Table 2, Channel 2 is nearly intrinsically doped so that it is fully depleted at equilibrium, providing a very sensitive transduction zone. Under these

circumstances, the response of Channel 2 is nonlinear, allowing for a very large amount of conductance modulation due to small variations in surface potential.

The 1 nm SiO_2 buffer layer around each SiC channel provides electrical isolation between the SiC channel and the cavity region where biomolecules are contained so that there is no direct charge transfer that would cause hysteresis or drift in the sensor response. Adjacent channels are spaced apart to allow for a nanocavity dimensioned 10 nm × 20 nm × 20 nm (L × W × H), while also accounting for a combined capture volume of about 4000 nm^3 for the immobilization of biomolecules.
The gate stack comprises a high-k hafnium dioxide (HfO_2) dielectric with a physical thickness of 2 nm that could be deposited via atomic layer deposition (ALD) on both inner sidewalls of the source and drain (Figure 2a). The dielectric constant of HfO_2 is $k \approx 23$ [31], and the equivalent oxide thickness (EOT) is approximately 0.39 nm. This results in exceptionally strong electrostatic coupling between the gate electrode and the channel regions while maintaining sufficient physical thickness to suppress direct quantum mechanical tunneling leakage. Dielectric modulation is expected to have increased sensitivity to changes in dielectric properties due to the use of a higher-k dielectric, which means that the change in cavity dielectric constant will yield larger percentage shifts in total gate capacitance and threshold voltage compared to using lower-k oxides. This principle of dielectric modulation has also been briefly discussed above.

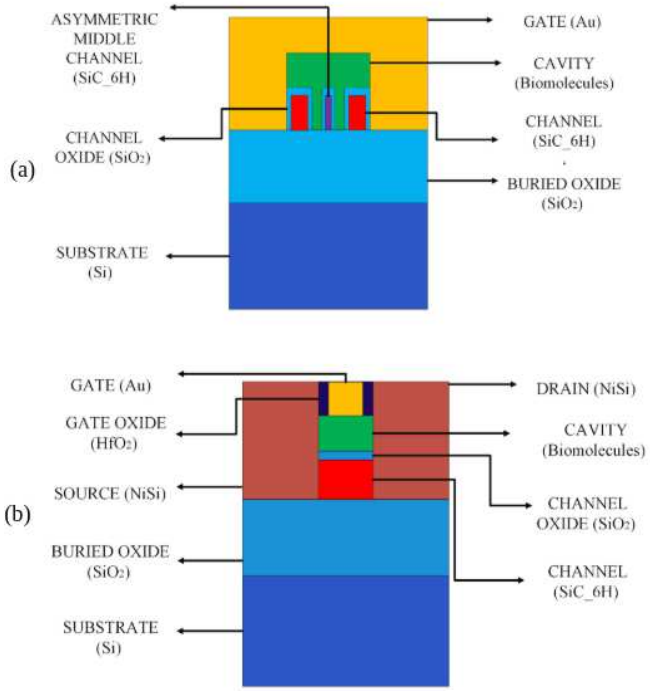


Fig. 2. **a)** X cross section **b)** Y cross section of the proposed asymmetric multichannel FinFET structure

The gate material used on this device is a 6-nm thick layer of gold (Au) having a work function of φ_m = 5.3 eV [32]. The use of gold for the gate was based on several practical considerations: (i) as an inert metal, gold is chemically stable and therefore will not corrode or undergo electrochemical reactions with the buffer solutions used in biological studies; (ii) gold provides very high levels of electrical conductivity, resulting in extremely low resistance to current flow at the gate, resulting in minimal delay caused by RC effects at the gate; and (iii) the work function of gold is properly aligned with the band structure of silicon carbide (SiC) to yield n-channel device threshold voltage (V_T) levels in the 0.8 to 1.2 V range. Also, the device utilizing the quasi-GAA structure will help reduce short channel effects, such as drain-induced barrier lowering (DIBL) and optimize gate control [33]. The electrodes surround the channel on three of its sides (top and both side walls), thus ensuring high electrostatic integrity for

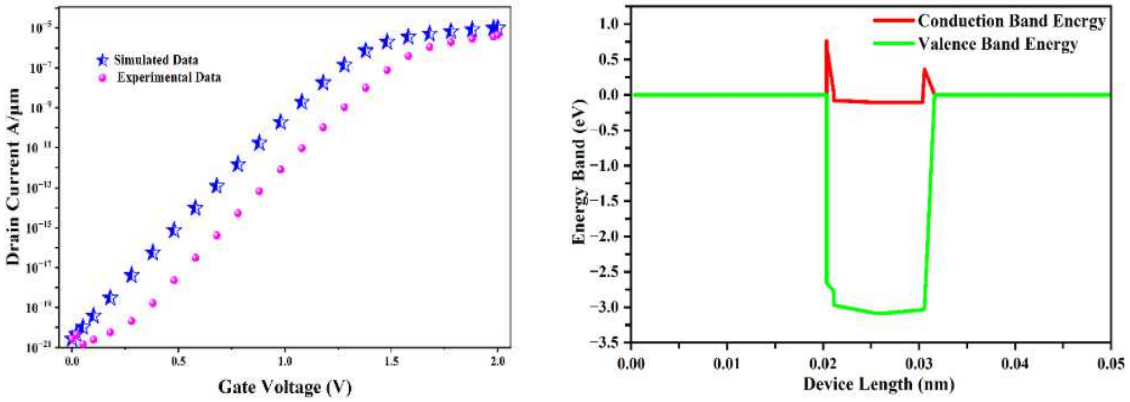
the device with 10 nm gate lengths (Fig. 2).
The biopolymer nanocavity is placed directly above the triple-channel stack and located between the two lateral HfO_2 gate dielectrics (Fig. 2). This placement ensures that changes in the cavity dielectric constant-induced by the binding of target cardiac biomarkers- directly modulate the electric field distribution in the channel depletion region, resulting in measurable shifts in threshold voltage and on/off current ratio.
All device simulations were performed on Synopsys Sentaurus TCAD (version 2020) with adaptive mesh generation (8-23 nm spacing) solving coupled semiconductor transport equations. Physics models including drift-diffusion with Fermi-Dirac statistics, Philips unified mobility (acoustic phonon, impurity, and surface roughness scattering), high-field saturation, Shockley-Read-Hall recombination, thermionic-field emission, were used in these simulations. They were run at 300 K with gate voltage swept 0-2 V (V_D = 0.4 V).
The target range of values was then added to the parameter in the S-Device tool on the workbench. Values of the cavity dielectric constant were varied from 1.0 to 3.5, representing cardiac biomarkers. Both uniform filling, as well as partial filling techniques were carried out to analyze the effects of partially filled cavity and compare the results. Device performance was compared with published conventional FinFET, negative capacitance FinFET, tunnel FET, and junction-less FinFET biosensors using various performance metrics such as sensitivity, on-off ratio, subthreshold swing, and fabrication complexity metrics. The proposed fabrication flow begins with SOI substrate preparation, followed by heteroepitaxial 6H-SiC growth with controlled doping (using buffer layers to mitigate lattice mismatch), EBL/EUV lithography for 10 nm patterning, thermal oxidation, sacrificial layer processing for cavity formation, ALD of HfO_2, gold gate deposition, and nickel silicidation.

III. RESULTS AND DISCUSSION

The performance of the proposed FinFET biosensor was evaluated through comprehensive TCAD simulations, focusing on the device's electrical and linearity response to various cardiac biomarkers.
By modulating the dielectric constant k within the cavity from 1.0 to 3.5- representing specific target molecules such as Uricase, and Cholesterol Oxidase (ChOx) - the impact of biomolecular presence was analyzed under both uniform (100%) and partial (50%) filling conditions. The earliest stages of our research revolved around looking at the electronic structure of the device itself, particularly in terms of the transmission of electricity along the surface to obtain a starting point from which we could measure. Following this initial investigation, we then looked at how we could change certain characteristics (ID-V_G), such as the V_{TH} and g_m, that would alter how well the device detects both positive and negative charge with respect to original values of I_{ON}/I_{OFF}. Finally, we assessed the reliability and linear performance of the device by using RF performance measures, specifically regarding the second and third-order Voltage Intercept Points (VIP_2, VIP_3) and the third-order Input Intercept Point (IIP_3).

The calibration study compared simulation results to their respective experimental counterparts (see Fig. 3(a)) to validate the efficacy of the developed simulation model [40]. The characteristics of the transfer function were investigated via a plot of drain current against gate voltage where both simulation and experimental data were found to closely follow a similar pattern over the entire range of gate voltages from 0-2V. Both data sets exhibited an increase in current with increasing gate voltages thereby indicating that the gate controlled the channel as expected. There was a small difference between the two datasets for drain currents at higher gate voltages but overall, it is clear that the results of the simulation reflect the electrical characteristics of the fabricated device. This close correlation between simulation and experimental results demonstrates the reliability of the proposed device model and validates its suitability for further performance analysis and device optimization. The conduction and valence bands energy distribution along the length of the channel under ON-state bias conditions (Fig.3 (b)) shows two peaks a pronounced one at the source-channel interface, with a peak barrier height of 0.76 eV corresponding to the NiSi-6H-SiC Schottky junction. The elevated barrier height is the result of the difference in work functions of the metal contact and wide-bandgap SiC channel as explained earlier. The suppressed thermionic emission and minimized OFF-state leakage currents are evident in

these results. Within the channel region the conduction band dips, indicating gate-induced barrier thinning and enhanced carrier injection through thermionic-field emission. This is the region of actively modulated sensing, where the changing dielectric constants in the nanocavity alter the surface potential and thus the tunnelling probability.



(a) (b)

Fig.3 (a) Calibration plot of the SBFinFET and **3(b)** Energy band diagram for the proposed SBFinFET biosensor

At the drain junction side, the conduction band peak is lower (0.36eV). The reduced barrier height here is explained by the asymmetric barrier modulation which is an advantageous feature for directional carrier transport and mitigating drain-induced barrier lowering (DIBL). The behavior of the valence band is similar, with a maintained intrinsic wide bandgap of 6H-SiC as indicated by the downward slope in the channel region. This shows that there is good electrostatic control of gates. The energy along the heavily doped contact regions is flat, and transitions across bands are very steep near the junctions, demonstrating excellent band alignment and low series resistance. The energy difference between the conduction and valence bands of the channel is roughly 3 eV, which is comparable to the intrinsic band gap of 6H-SiC (3.03 eV). In addition to this, the conduction band peak at the source-side (~0.76 eV) is also similar to the theoretical value for the NiSi/SiC Schottky barrier height (~0.95 eV), while the lower barrier on the drain-side indicates that there is barrier thinning caused by how we are biasing the device and the asymmetry of transport. All of this would suggest that there is a potential for improved signal discrimination and ON/OFF ratios.

The lateral electric field profile of SB-FinFET biosensor in the ON-state can be seen in Fig. 4. There is one main peak (~9 x 10^5) at the source-channel interface (x = 20 nm) caused by the NiSi/SiC Schottky junction. The localized nature of this field allows for a smaller tunneling barrier at the source-side, which increases the efficiency of carrier injection through thermionic-field emission. There is a second peak of moderate magnitude at the drain junction (x = 30 nm) indicating that the barrier can be tuned and drain-induced barrier lowering (DIBL) can be successfully mitigated. The field exhibits high sensitivity to dielectric variations inside the central nanocavity, allowing for precise surface potential control. The local field distribution and surface potential are modified by the introduction of biomolecules with different dielectric constants modifies, hence directly modulating the tunneling probability and channel conductance. This spatial decoupling-where contact fields manage injection and the central field manages sensing- explains the device's superior I_{ON}/I_{OFF} ratio and its sensitivity toward low-k cardiac biomarkers.

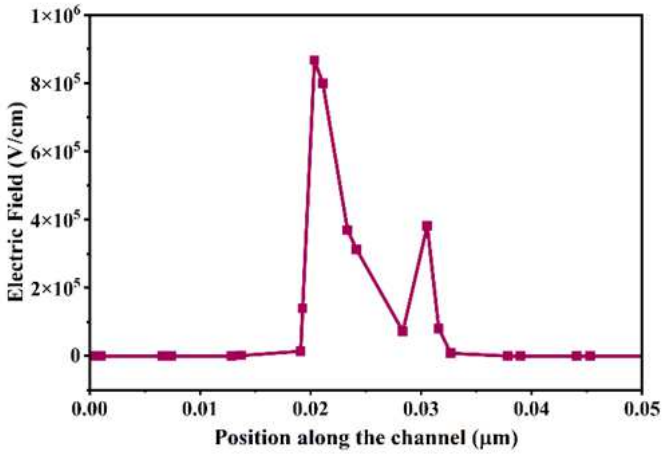


Fig.4. Electric field distribution along the channel length of the proposed asymmetric triple-channel SB-FinFET biosensor

Fig. 5. compares the electrostatic potential profiles along the channel of the proposed asymmetric triple-channel SB-FinFET and a standard single-channel reference under identical bias. It is observed that both architectures show a sharp potential rise at the source–channel interface, due to the Schottky barrier modulation and gate-induced bending. However, the triple-channel design achieves a higher peak potential and a more pronounced gradient. This enhancement is due to the superior electrostatic coupling and a larger effective surface area. Therefore, the intensified field penetration into the central sensing region allows for more effective dielectric modulation for biosensing. The triple-channel device also exhibits improved potential stability toward the drain showing enhanced resistance to DIBL and short-channel effects compared to the weaker gate control observed in the single-channel counterpart.

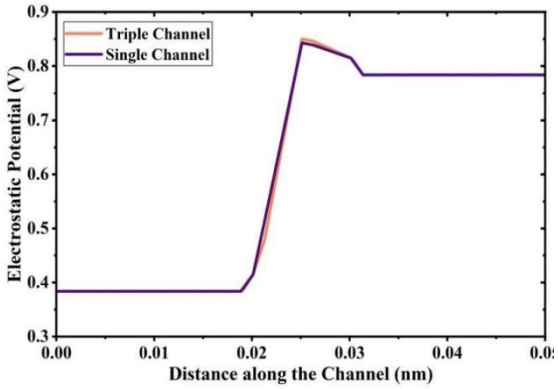
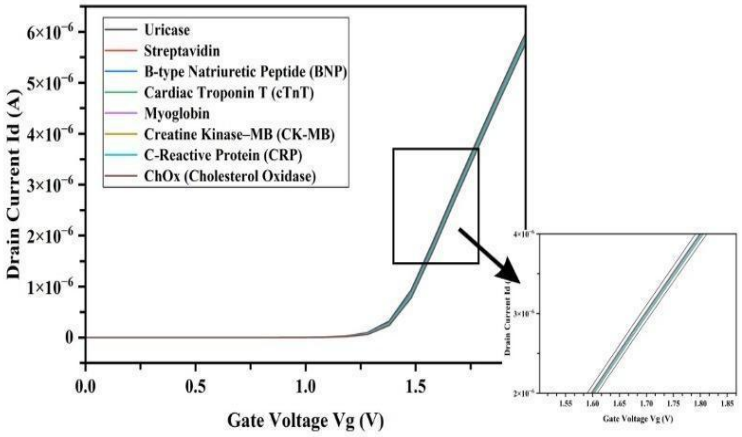


Fig.5. Comparison of the electrostatic potential distribution along the channel length for the proposed asymmetric triple-channel SB-FinFET and a conventional single-channel device

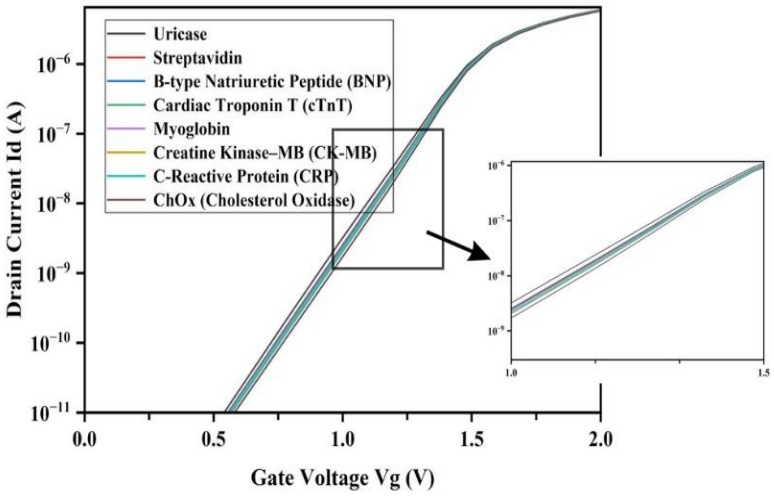
The linear and semi-logarithmic transfer characteristics of the proposed triple-channel SB-FinFET biosensor for various biomolecular targets are depicted in Fig.6. Noticeable shifts in the I_d-V_g characteristics are evident, signifying successful modulation of the channel conductance based on biomolecule-mediated dielectric modulation in the sensing cavity.

In the subthreshold regime, pronounced threshold voltage shifts are achieved with minimal variation in

the subthreshold slopes for all scenarios, signifying robust gate electrostatic control with insignificant compromise in device integrity. It is observed that with higher dielectric constant, the threshold voltage decreases, that is, the device turns on earlier because the effective gate capacitance increases and the field penetrates more strongly into the channel. The largest variation appears in the subthreshold region, since the drain current here depends exponentially on surface potential. The triple-channel stacked configuration and asymmetrical doping profile enable improved sensing resolution through the synergistic integration of high drive current and strong electrostatic control. These experimental findings validate the proposed device's efficacy for label-free detection and differentiation of multiple cardiac biomarkers at the nanoscale.



(a)



(b)

Fig.6. a) Linear and **b)** Log plots of Drain current (Id - Vg) for different biomolecules

Fig. 7 is an illustration of the varying I_{ON}/I_{OFF} ratio of the proposed asymmetric triple-channel SB-FinFET biosensor as a function of the dielectric constant (k) of the biomolecules occupying the sensing cavity. As k rises from 1.5 to 3.5, the ratio is seen to monotonically increase, with value improving from approximately 5.9×10^8 to beyond 6.6×10^8. This is due to stronger electrostatic gate coupling between the gate electrode and the channel as the effective cavity permittivity increases. Biomolecules with

higher k intensify the local electric field penetration into the highly doped central sensing channel. This results in more pronounced barrier thinning at the source junction and higher ON-current. The OFF current remains almost unchanged due to the inherent SB suppression. This asymmetric modulation leads to a noticeable improvement in the current-gain behavior, reflected not only in the elevated I_{ON}/I_{OFF} ratio but also in the increase of the current sensitivity metric as will be discussed further. Because the rise in the plotted line is gradual and not instantaneous or severe, it indicates that there is good electrostatic control with no large changes in the amount of electrical leakage. Also, this indicates that the Switchable Device can switch reliably at high values of the dielectric constant.

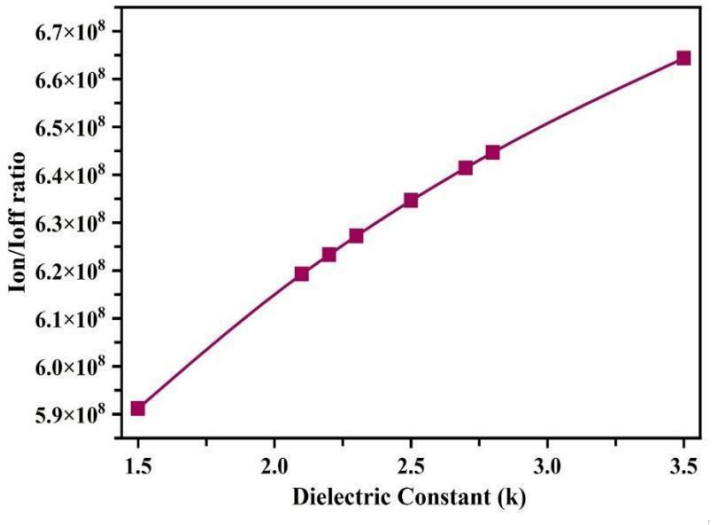


Fig. 7. I_{ON}/I_{OFF} ratio for biomolecules with different dielectric values

Sensitivity is an important parameter used to assess the performance and functionality of biosensors when determining the presence of biomolecules. The following equation can be used to quantify sensitivity based on calculated I_{ON}/I_{OFF} values:

$$S_{\frac{I_{ON}}{I_{OFF}}} = \left(\frac{\frac{I_{ON}}{I_{OFF(BC)}} - \frac{I_{ON}}{I_{OFF(air)}}}{\frac{I_{ON}}{I_{OFF(air)}}} \right) \qquad (1)$$

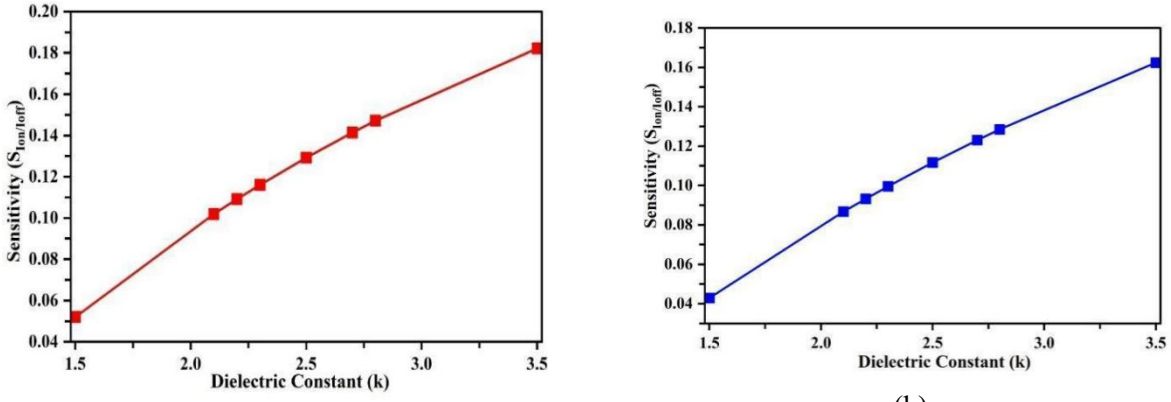


Fig. 8. Variaton of I_{ON}/I_{OFF} sensitivity for (a) positively and (b) negatively charged doping of channels against the dielectric constant of biomolecules inserted in the cavity

The observed response is a result of the combined effect from the dielectric permittivity of the biomolecule and high-k HfO_2 gate oxide, which produces a higher electric field penetration into the

lightly doped sensing region. Consequently, the modulation of surface potential due to the dielectrically created charge leads to measurable changes in the relative magnitude of I_{ON}/I_{OFF} through distinct threshold-shift voltages. It should be noted that the low-k range common to cardiac biomarkers provides only minute increments in sensitivity, but the consistency of the observed trends demonstrates that this device can provide high-resolution discrimination in very narrow dielectric ranges, while still providing very stable I_{OFF} characteristics. Fig. 9 shows the transconductance variation according to gate voltage, and the formula for its calculation is given below.

$$g_m = \frac{\partial ID}{\partial V_G} \qquad (2)$$

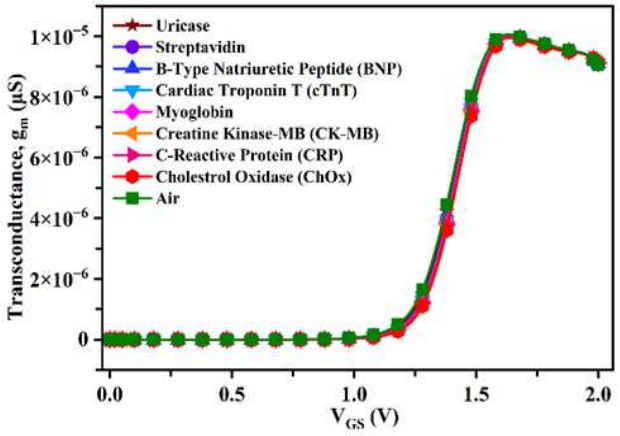


Fig. 9. Transconductance (g_m) vs. V_G characteristics of the FinFET biosensor for different biomolecules under dielectric modulation.

In practice, biosensing can be impeded by steric effects, diffusion, and immobilization. This makes it difficult to achieve a fully occupied nanocavity. Hence, the functionality of this device when partially filled is crucial. In this work, the Fill Factor (FF) is defined as follows:

$$FF(\%) = \left(\frac{\text{Area of nano}-\text{cavity occupied by biomolecules}}{\text{Total area of nano}-\text{cavity}}\right) \times 100 \qquad (3)$$

Two representative cases are compared in this regard: 50% and 100% FF. Fig.10 illustrates the sensitivity variation across the dielectric range for both configurations. Although the 100% FF case consistently provides higher sensitivity because of the maximum dielectric modulation and improved field penetration, the 50% FF case provides a similar monotonic variation. Therefore, although partial filling decreases the permittivity contrast- hence slightly reducing the gate–channel coupling and drain current modulation (ΔI_D) - the architecture is still reliable for biomolecule detection. This stability is quite useful for clinical applications where optimal cavity usage is not always guaranteed. Although this work does not focus on simulating binding kinetics, the relationship between the fill factor and sensitivity provides a semi-quantitative estimate for biomolecule concentration. Since partial filling of the cavity leads to a corresponding reduction in electrostatic modulation, the device provides a means for concentration-dependent trend analysis. This suggests that the sensor can provide information on relative variations in biomarker concentration, even if absolute quantification is not the main concern.

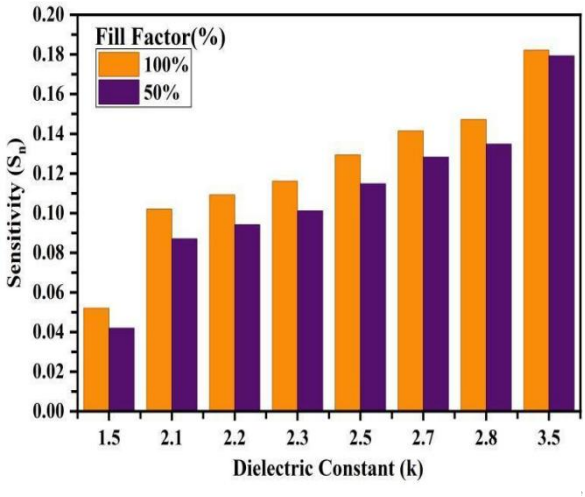


Fig. 10. Comparison of Sensitivity for different cavity fill factors

Fig. 11 illustrates the variation threshold voltage (V_{TH}) with the biomolecule dielectric constant. As k increases from 1.5 to 3.5 V_{TH} exhibits a monotonically increases from approximately 1.32 V to 1.36 V. This variation is due to dielectric-induced modulation of the effective gate capacitance, which in turn distributes the electric field within the central sensing channel. The higher dielectric constant results in stronger gate-channel coupling and modulates the surface potential in the source region; namely, a stronger electrostatic control command is required to accomplish the required band bending and barrier thinning for channel inversion due to the higher gate voltage. The systematic and controlled variation of this V_{TH} guarentees robust discrimination of low-k cardiac biomarkers while maintaining high switching integrity and noise immunity.

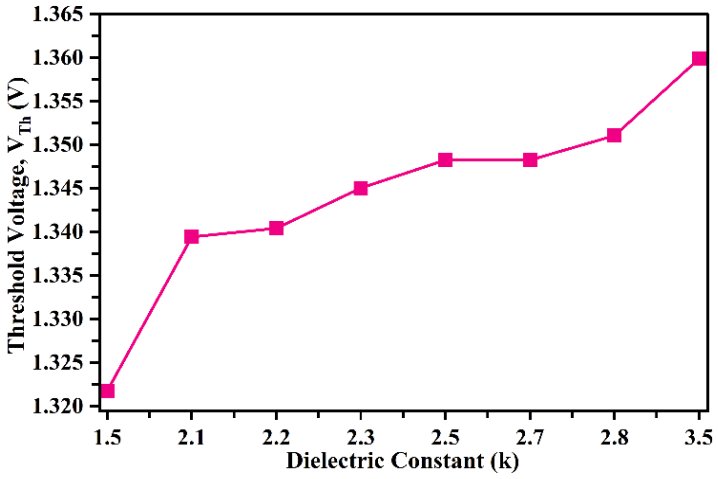


Fig. 11. Variation of threshold voltage (V_{TH}) of the proposed SB-FinFET biosensor as a function of the dielectric constant (k) of biomolecules

In Fig.12 the third-order transconductance coefficient (g_{m3}) versus gate-to-source voltage (V_{GS}) is shown to assess the linearity and distortion profiles of the proposed SB-FinFET. G_{m3} is a third-order derivative of drain current, and a metric used for quantifying higher-order nonlinearity. Lower absolute magnitudes of g_{m3} can mean enhanced signal fidelity and reduced harmonic distortion. In the subthreshold and weak-inversion regimes, g_{m3} remains near zero for all biomolecules, meaning negligible nonlinear effects at low bias. However, a localized positive peak emerges near the onset of

strong inversion, followed by a sign reversal and a negative trough at higher $V_{GS.}$ These observations are in agreement with the rapid injection of carriers into SB-FinFETs due to the thin source-junction barriers. Although the value for g_{m3} is small (approximately 10^{-4} mA/V³), the nonlinear response of the device is very well controlled. The curves are also very closely grouped, which suggests that dielectric modulation does not produce a significant amount of high-order distortion and the device will provide a reliable amplification of the signal with a high SNR for biosensing.

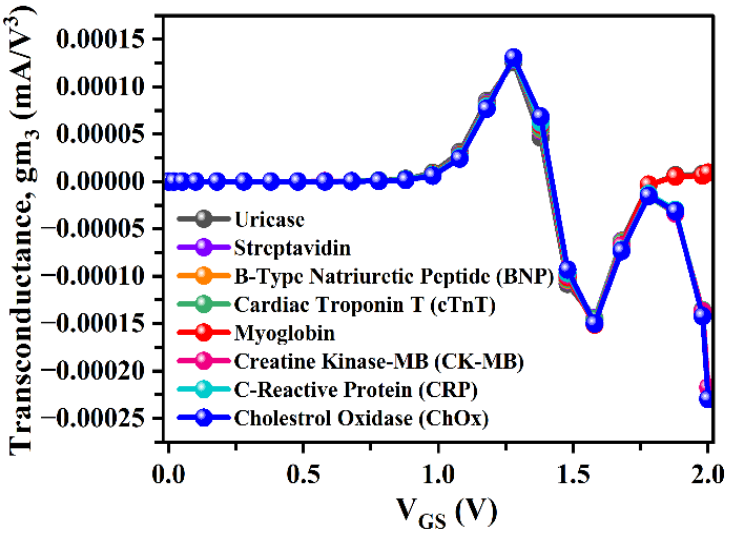


Fig. 12. Third-Order Transconductance (g_{m3}) for different biomolecules in the nanocavity

Fig. 13 demonstrates how the second-order voltage intercept point (VIP_2) varies as a function of V_{GS} for the proposed asymmetric triple-channel SB-FinFET biosensor. VIP_2 is widely used as an indicator of the amount of even-order nonlinear distortion that exists within the system level and has been studied in great detail for asymmetric layouts because of the imbalance caused by an asymmetric device, and therefore cannot inherently cancel out second-order harmonics. The equation representing this parameter is as follows [37].

$$VIP_2 = 4 \times \left(\frac{g_m}{g_{m2}}\right) \quad (4)$$

Based on the analysis of the data obtained from this device, it is clear that in both the low-bias and moderate inversion regions, the VIP_2 values from the majority of the biomolecules are located very close to the origin. This means that the even-order distortion will be relatively insignificant, and there is excellent electrostatic control. With an increase in the gate voltage, peaks can be found that correspond to localized distortions wherein some biomolecules exhibit steep peak to peak transitions, while others do not. The peak regions correspond to the extremely fast carrier injection and barrier control effect occurring around the strongest inversion region. While localized characteristics do exist, the VIP_2 trends clearly show that the asymmetrical channel design results in an acceptable level of second order linearity while still allowing for high efficiency with dielectric based sensing. The permittivity changes induced by the biomolecules do not affect the performance of the even order distortion at all as can be seen by the tightly packed curves.

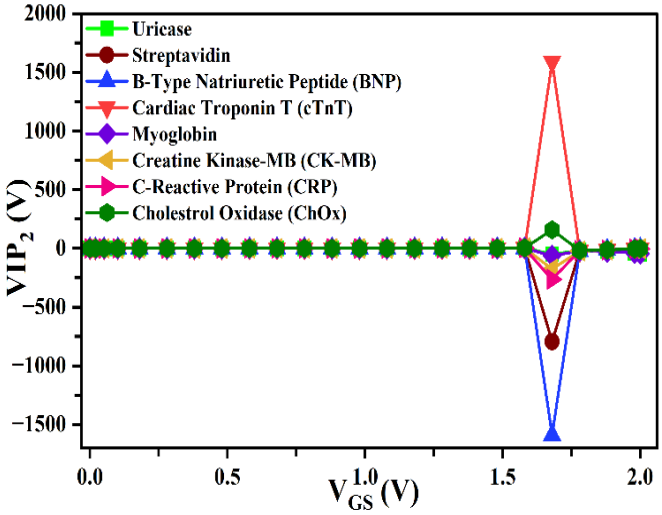


Fig. 13. Second-order voltage intercept point (VIP_2) of the proposed SB-FinFET biosensor for different cardiac biomolecules

The VIP_3 (third-order voltage intercept point), critical for characterising the odd-order nonlinear distortion component of a device, is shown in Fig. 14. This information is derived as follows [38].

$$VIP_3 = 24 \times \sqrt{\left(\frac{g_m}{g_{m3}}\right)} \quad (5)$$

In sub-threshold and weak inversion conditions VIP_3 is found to be low and static. This indicates that third-order signal interference does not occur at low bias currents. The increase in bias current applied to the device increases the gate-source voltage above the threshold voltage, which results in much higher VIP_3 values as a result of improved carrier transport (due to the increased electric field) and more nonlinear channel conductance. The amount of separation between the VIP_3 curves for each of the biomolecules studied is enhanced by using higher bias current (i.e. dielectric-dependent modulation of the gate capacitance and the internal electric field). However, the VIP_3 values are still within acceptable ranges. The results imply that the device can effectively measure biomolecules while continuing to maintain effective odd-order linearity in its output.

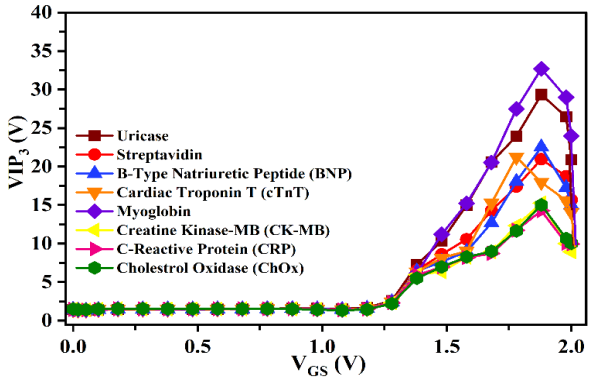


Fig. 14. Third-order voltage intercept point (VIP_3) for various biomolecules in the proposed SB-FinFET

The third-order input intercept point (IIP_3) is depicted in Fig 15, which indicates the theoretical voltage into the transistor at which the third-order intermodulation product intersects with the fundamental signal's voltage on the input side. The formula used to calculate IIP3 is as follows [38]:

$$IIP_3 = \frac{2}{3} \times \left(\frac{g_m}{g_{m3\ \mathrm{Rs}}}\right) \qquad (6)$$

The IIP_3 values remain near 0 in the subthreshold region, indicating a high degree of signal integrity, even for low-bias excitation, and serve as a reference point for input-referred linearity and distortion immunity. In the vicinity of when strong inversion begins, there will be an extreme dip before the curve steeply increases. This phenomenon can be explained by transients being present due to curvature in the transconductance and by the nonlinear nature of the Schottky-based carrier injection. Though they occur at higher levels of gate bias, the IIP3 values are very insensitive to the sensing window. This condition implies that the dielectric modulation method can provide improved sensitivity while retaining good input linearity, which allows the proposed SB-FinFET device to achieve a balanced compromise between signal resolution and low noise operation.

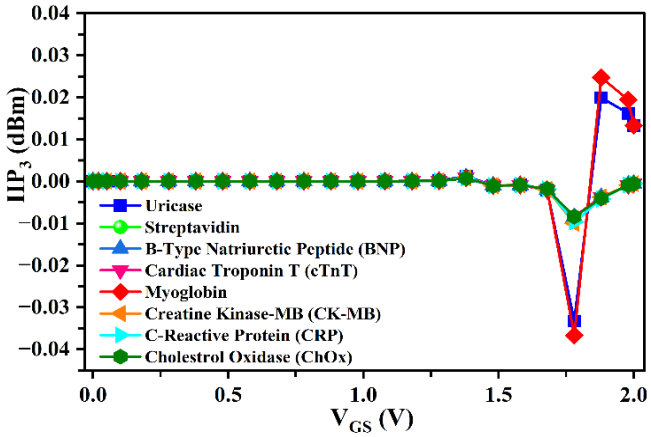


Fig. 15. Third-order input intercept point (IIP_3) variation for different biomolecules in SB-FinFET

Table 3: Comparison of the obtained parameters of the proposed asymmetric triple-channel SB-FinFET biosensor with existing literature

S.No.	Biosensor Configuration	k	Transconductance (g_m)	I_{ON}/I_{OFF}	I_{ON} (A/µm)	Reference
1	**DM RSD NC-FINFET**	4.7	7.68×10^{-5}	2.39×10^{4}	5×10^{-4}	[6]
2	**GaAs FinFET**	3.52	4×10^{-5}	1×10^{8}	16×10^{-6}	[8]
3	**TF-FinFET**	3.57	2×10^{-4}	10^{3}	10^{-5}	[20]

4	**DM-JL MOSFET**	5	-	10^{7}	8×10^{-5}	[39]
5	**Proposed multichannel SB-FinFET**	3.5	1×10^{-5}	6.65×10^{8}	6×10^{-6}	This work

Table 3 presents a comparison of the proposed multichannel Schottky-barrier FinFET (SB-FinFET) biosensor with previously reported biosensor configurations in terms of dielectric constant (k), transconductance (g_m), I_{ON}/I_{OFF} ratio, and ON-state current (I_{ON}). The proposed SB-FinFET uses a dielectric constant of 3.5 and exhibits a transconductance of (10^{-5}) S, indicating effective gate control over the channel. It achieves a high I_{ON}/I_{OFF} ratio of (6.65×10^{8}), which indicates a strong distinction between the ON and OFF states and is beneficial for biosensing applications. Although the I_{ON} value of (10^{-6}) A/μm is lower than that of some reported devices, the proposed device provides a high I_{ON}/I_{OFF} ratio along with a multichannel configuration, demonstrating its potential for sensitive and reliable biomolecule detection. Overall, the comparison confirms that the proposed SB-FinFET offers competitive electrical characteristics compared with existing biosensor structures.

IV. CONCLUSION

A novel type of biosensor called a Dielectric-Modulated Asymmetrical (DMA) Triple-Channel Schottky-Barrier FinFET (SB-FinFET) has been developed to improve low-dielectric cardiac biomarker sensing with k-values ranging from about 1.5 to 3.5. The device integrates NiSi Schottky contacts, a 6H-SiC, wide-bandgap channel material, and a high-k HfO_2 gate stack into a multi-channel configuration that solves the traditional trade-off between sensor sensitivity and current-driving capability. The ultra-narrow, lightly doped central channel provides a highly sensitive transduction mechanism; the moderately doped outer channels supply enough ON-state current to electrically detect the target biomarker. Simulation studies conducted with 3D TCAD show that this biosensor can achieve an $I_{ON}/I_{OF}F$ ratio greater than 10^{8}, excellent sub-threshold performance, and significantly different transconductance values, and threshold voltages, among the various cardiac biomarkers. In addition, the dielectric modulation effect exhibited well-behaved, monotonic behavior over both full and partial cavity fill factors, indicating that the device would be insensitive to non-ideal sensing conditions. Several higher-order linearity performance metrics, including gm_3, VIP_2, VIP_3, and IIP_3, were evaluated for the biosensor, with reductions in nonlinear distortion noted, thus improving the device's sensitivity without degrading its signal purity.

A comparison of the SB-FinFET device to several currently commercially available devices such as junction-less devices, Tunnel-FETs, and Negative Capacitance devices shows that the SB-FinFET exhibits comparable or better performance. Additionally, the functionalisation of the biomarkers within the device will provide low-k biomarker detection without requiring biochemical functionalisation. The results of the research provide an initial design basis for optimising the design for subsequent experimental implementation. The next steps will involve expanding the study's findings by performing a physical implementation of the device, performing nanocavity functionalisation, and validating the findings through experimentation in wet biological environments to evaluate the effects of ionic screening and binding kinetics. More research is needed to develop sensor arrays that enable multiplexed detection capability, perform noise modelling, and co-design circuitry in order to enable portable diagnostics. Emphasis on cardiac-specific biomarkers is extremely relevant as the rapid and highly sensitive detection of proteins such as Troponin or Myoglobin will dramatically decrease the time to diagnosis in a clinical setting. The end goal of this project is to develop a framework based on electrostatics that is valid when evaluating target molecules at low-dielectric properties. The framework should serve as the link between traditional FET biosensors, and specialized cardiac nanoelectronics.

We propose to develop an asymmetric triple-channel SB-FinFET design, which is a scalable, CMOS compatible device that enables both increased electrostatic control and enhancement of the total signal while simultaneously reducing leakage. Thus, this is a high resolution platform for label-free sensing of cardiac biomarkers.

Supplementary information. NA
Acknowledgments. NA
Declarations
• Funding -No
• Conflict of interest/Competing interests -No
• Ethics approval -NA
• Consent to participate-NA
• Consent for publication-Yes
• Availability of data and materials- Yes
• Code availability -Yes

Authors' contributions- Radhika P and Lakshita K J conceived the overall research idea. Radhika P and Shalini Virumandi conducted the virtual simulation experiments and generated the data. The remaining authors contributed to data management, validation, and provided guidance on research concepts. Radhika P drafted the manuscript, while Prayag Sharma, Ravi Tiwari, and Prashanth Kumar developed the methodology. All authors reviewed and approved the final version of the manuscript.

FUNDING

No Funding for this work

CONFLICT OF INTEREST

The authors declare that they have no conflicts of interest.

DATA AVAILABILITY STATEMENT

All data generated or analysed during this study are included in this published article

REFERENCES

1. World Health Organization, Cardiovascular diseases (CVDs), WHO Fact Sheets. Available: https://www.who.int/news-room/fact-sheets/detail/cardiovascular-diseases-(cvds). Accessed June 30, 2026.
2. S. Saheera, Indian Heart J. **75**, 91–97 (2023). https://doi.org/10.1016/j.ihj.2023.01.011
3. N. Midhun, J. Sonia Bai, K. Chakrapani, Haripriya, C. K. V. S. Pathuri, and N. S. Ramalakshmi, Indian J. Microbiol. Res. **8**, 10–14 (2021). https://doi.org/10.18231/j.ijmr.2021.003
4. P. Ramesh, Malvika, and B. Choudhuri, B. Mater. Sci. Eng. **310**, 117727 (2024). https://doi.org/10.1016/j.mseb.2024.117727
5. K. N. Priyadarshani, S. Singh, and M. K. A. Mohammed, Inorg. Chem. Commun. **148**, 110350 (2023). https://doi.org/10.1016/j.inoche.2022.110350
6. A. Dixit, D. P. Samajdar, and V. Chauhan, IEEE Trans. Electron Devices **68**, 5204–5210 (2021). https://doi.org/10.1109/TED.2021.3107368

7. H. D. Sehgal, Y. Pratap, M. Gupta, and S. Kabra, in Proc. Int. Conf. Power Electron., Control Autom. (ICPECA) (New Delhi, India, 2019), pp. 1–6. https://doi.org/10.1109/ICPECA47973.2019.8975506
8. M. H. Manzoor, A. Ray, and A. Naugarhiya, in Proc. 2nd Int. Conf. Paradigm Shifts Commun. Embedded Syst., Mach. Learn. Signal Process. (PCEMS) (Nagpur, India, 2023), pp. 1–6. https://doi.org/10.1109/PCEMS58491.2023.10136113
9. H. D. Sehgal, Y. Pratap, M. Gupta, and S. Kabra, IEEE Sensors J. **21**, 18897–18904 (2021). https://doi.org/10.1109/JSEN.2021.3090263
10. K. Shoorideh and C. O. Chui, IEEE Trans. Electron Devices **59**, 3104–3110 (2012). https://doi.org/10.1109/TED.2012.2214221
11. M. Aditya, K. S. Rao, and B. Balaji, Silicon **14**, 8269–8276 (2022). https://doi.org/10.1007/s12633-021-01638-8
12. S. Gupta, Y. Pratap, and M. Gupta, in Proc. 7th Int. Conf. Electron., Mater. Eng. Nano-Technol. (IEMENTech) (Kolkata, India, 2023), pp. 1–5. https://doi.org/10.1109/IEMENTech60402.2023.10423543
13. A. Dixit, D. P. Samajdar, and N. Bagga, in Proc. IEEE INDICON (2021), pp. 1–5. https://doi.org/10.1109/INDICON52576.2021.9691731
14. A. Lamba, R. Chaujar, and M. J. Deen, Micro Nanostruct. **205**, 208177 (2025). https://doi.org/10.1016/j.micrna.2025.208177
15. Gandhi, Navneet and Rathore, Sunil and Jaisawal, Rajeewa Kumar and Kondekar, P. N. and Dixit, Ankit and Kumar, Naveen and Georgiev, Vihar and Bagga, Navjeet, IEEE Trans. Dielectr. Electr. Insul. **32**, 1575–1582 (2025). https://doi.org/10.1109/TDEI.2024.3504407
16. P. K. Swain, D. Nayak, P. K. Rout, and S. M. Biswal, in Proc. IEEE Int. Conf. Electron Devices Soc. Kolkata Chapter (EDKCON) (Kolkata, India, 2024), pp. 333–336. https://doi.org/10.1109/EDKCON62339.2024.10870792
17. Xu, Xiaorui and Deng, Yicong and Li, Titao and Xu, Xiaohui and Yang, Dan and Zhu, Minmin and Zhang, Haizhong and Lu, Xiaoqiang, IEEE Trans. Electron Devices **71**, 2530–2535 (2024). https://doi.org/10.1109/TED.2024.3365078
18. Y. S. Nagarjuna, P. R. Kumar, and M. D. Prakash, in Proc. Global Conf. Emerging Technol. (GINOTECH) (Pune, India, 2025), pp. 1–4. https://doi.org/10.1109/GINOTECH63460.2025.11076817
19. R. Saha, Y. Hirpara, and S. Hoque, IEEE Trans. Nanotechnol. **20**, 552–560 (2021). https://doi.org/10.1109/TNANO.2021.3093927
20. H. Gudaghe, M. Kashyap, and R. Chaujar, in Proc. Devices Integr. Circuit (DevIC) (Kalyani, India, 2021), pp. 45–49. https://doi.org/10.1109/DevIC50843.2021.9455938
21. S. Verma, S. L. Tripathi, V. Narula, B. Raj, and N. Sahota, in Proc. IEEE Int. Conf. Electron Devices Soc. Kolkata Chapter (EDKCON) (Kolkata, India, 2024), pp. 77–82. https://doi.org/10.1109/EDKCON62339.2024.10870605
22. P. Kumar, A. Vinod, B. Jena, A. Arivarasi, and J. Bahadur, Int. J. Numer. Model. Electron. Netw. Devices Fields. **32**, (2024). https://doi.org/10.1002/jnm.3291
23. P. Kumar, Papanasam Esakki, Lucky Agarwal, PeddaKrishna, Sumit Kale & Brinda Bhowmick, Silicon **15**, 25–35 (2023). https://doi.org/10.1007/s12633-022-01994-z
24. Langpoklakpam, Catherine, An-Chen Liu, Kuo-Hsiung Chu, Lung-Hsing Hsu, Wen-Chung Lee, Shih-Chen Chen, Chia-Wei Sun, Min-Hsiung Shih, Kung-Yen Lee, and Hao-Chung Kuo, Crystals **12**, 245 (2022). https://doi.org/10.3390/cryst12020245
25. S. E. Saddow, C. Coletti, C. L. Frewin, A. Oliveros, M. Jarosezski & N. Schettini, MRS Online Proc. Libr. **1246**, B08-08 (2009). https://doi.org/10.1557/PROC-1246-B08-08
26. Y. Pathak, B. D. Malhotra, and R. Chaujar, J. Mater. Sci.: Mater. Electron. **33**, 13558–13567 (2022). https://doi.org/10.1007/s10854-022-08290-x
27. C. Lavoie, F. M. d'Heurle, C. Detavernier, and C. Cabral, Microelectron. Eng. **70**, 144–157 (2003). https://doi.org/10.1016/S0167-9317(03)00380-0

28. S. Y. Davydov, A. A. Lebedev, and O. V. Posrednik, Semiconductors **39**, 1391–1393 (2005). https://doi.org/10.1134/1.2140310
29. S. Y. Davydov, Semiconductors **41**, 696–698 (2007). https://doi.org/10.1134/S1063782607060152
30. Y. Y. Lebedinskii and A. V. Zenkevich, Microelectron. Reliab. **47**, 649–652 (2007). https://doi.org/10.1016/j.microrel.2007.01.064
31. Taeho Kang, Joonho Park, Hanggyo Jung, Haeju Choi, Sang-Min Lee, Nayeong Lee, Ryong-Gyu Lee, Gahye Kim, Seung-Hwan Kim, Hyung-jun Kim, Cheol-Woong Yang, Jongwook Jeon, Yong-Hoon Kim, Sungjoo Lee, Adv. Mater. **36**, 2312747 (2024). https://doi.org/10.1002/adma.202312747
32. W. M. H. Sachtler, G. J. H. Dorgelo, and A. A. Holscher, Surf. Sci. **5**, 221–229 (1966). https://doi.org/10.1016/0039-6028(66)90083-5
33. Loubet, N. and Hook, et al., in Proc. Symp. VLSI Technol. (Kyoto, Japan, 2017), pp. T230–T231. https://doi.org/10.23919/VLSIT.2017.7998183
34. Wenjie Zhao, Jiawei Hu, Jinlong Liu, Xin Li, Sheng Sun, Xiaofeng Luan, Yang Zhao, Shuhua Wei, Mingxiao Li, Qingzhu Zhang & Chengjun Huang, Microsyst. Nanoeng. **8**, 57 (2022). https://doi.org/10.1038/s41378-022-00387-x
35. R. Hao, L. Liu, J. Yuan, L. Wu, and S. Lei, Biosensors **13**, 426 (2023). https://doi.org/10.3390/bios13040426
36. B. Smaani, F. Nafa, M. S. Benlatrech, I. Mahdi, H. Akroum, M. W. Azizi, K. Harrar, and S. Kanungo, Beilstein J. Nanotechnol. **15**, 977–994 (2024). https://doi.org/10.3762/bjnano.15.80
37. R. K. Jaisawal, S. Rathore, P. N. Kondekar, and N. Bagga, IEEE Trans. Nanotechnol. **22**, 545–551 (2023). https://doi.org/10.1109/TNANO.2023.3308814
38. V. Shalini and P. Kumar, Micro Nanostruct. **199**, 208078 (2025). https://doi.org/10.1016/j.micrna.2025.208078
39. Ajay, R. Narang, M. Saxena, and M. Gupta, Superlattices Microstruct. **85**, 557–572 (2015). https://doi.org/10.1016/j.spmi.2015.04.040
40. S. R. Kola and Y. Li, Processes. **13**, 3103 (2025). https://doi.org/10.3390/pr13103103